Langmuir

ARTICLE

pubs.acs.org/Langmuir

Novel Route to Size-Controlled Fe−MIL-88B−NH_2 Metal−Organic Framework Nanocrystals

Minh-Hao Pham,[†] Gia-Thanh Vuong,[†] Anh-Tuan Vu,[‡] and Trong-On Do*[,†]

[†]Department of Chemical Engineering, Laval University, Quebec City, Quebec G1V 0A6, Canada

[‡]Institute of Chemistry, Vietnamese Academy of Science and Technology, Building A18, 18 Hoang Quoc Viet, Cau Giay, Hanoi, Vietnam

Supporting Information

ABSTRACT: A new approach for the synthesis of uniform metal−organic framework (MOF) nanocrystals with controlled sizes and aspect ratios has been developed using simultaneously the non-ionic triblock co-polymer F127 and acetic acid as stabilizing and deprotonating agents, respectively. The alkylene oxide segments of the triblock co-polymer can coordinate with metal ions and stabilize MOF nuclei in the early stage of the formation of MOF nanocrystals. Acetic acid can control the deprotonation of carboxylic linkers during the synthesis and, thus, enables the control of the rate of nucleation, leading to the tailoring of the size and aspect ratio (length/width) of nanocrystals. Fe−MIL-88B−NH_2, as an iron-based MOF crystal, was selected as a typical example to illustrate our approach. The results reveal that this approach is used for not only the synthesis of uniform nanocrystals but also the control of the size and aspect ratio of the materials. The size and aspect ratio of nanocrystals increase with an increase in the concentration of acetic acid in the synthetic mixture. The non-ionic triblock co-polymer F127 and acetic acid can be easily removed from the Fe−MIL-88B−NH_2 nanocrystal products by washing with ethanol, and thus, their amine groups are available for practical applications. The approach is expected to synthesize various nanosized carboxylate-based MOF members, such as MIL-53, MIL-89, MIL-100, and MIL-101.

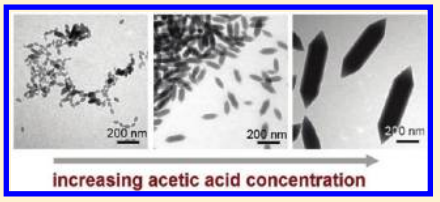

INTRODUCTION

Metal−organic frameworks (MOFs) are crystalline porous materials whose structure is composed of metal-oxide units joined by organic linkers through strong covalent bonds. These materials exhibit high surface areas (up to 6500 $m^2\ g^{-1}$) and high pore volumes (1−2 $cm^3\ g^{-1}$) and are of considerable interest for many potential applications.[1,2] However, because of their microporosity (generally, pore size of <2 nm), the potential applications of these materials are limited. To overcome this limitation, as in the case of microporous zeolites,[3,4] one can either create mesopore channels within MOF crystals or reduce the crystal to nanosize. Attempts have been made to synthesize porous MOFs with large pore diameters in the range of 2−50 nm.[5−7] For example, MIL-101[5] and UMCM-2[6] exhibit mesoporous behavior, owing to mesoporous cages found throughout the structures; however, the mesopores are often restricted by small apertures that prohibit large molecules from accessing the space inside. Increasing the length of the organic linker is another option, but with few exceptions,[8] MOFs built up from long linkers tend to collapse upon guest removal[9] or form catenated structures.[10] Recently, the synthesis of hierarchically micro- and mesoporous MOF materials in an ionic liquid/supercritical CO_2/surfactant emulsion system was reported.[11] These materials combine advantages of both meso- and micropores and have potential applications in gas separation and catalysis.

Recently, nanoscale MOF crystals have emerged as important candidates with a significant impact for drug delivery,[12] biomedical imaging applications,[13,14] chemical sensing,[15] and gas separation,[16] owing to easier transport of guest molecules through nanosize, short diffusion pathways and exposed active sites within MOF nanocrystals.[17,18] Furthermore, the external surface of MOF nanocrystals also offers the ability to functionalize core−shell nanostructures for biomedical sensing and imaging.[19] The adsorbate-induced structural flexibility of some MOFs, in which the unit cell parameters can vary significantly when the guests are adsorbed within their pores, enables the induction of stress at the interfaces between MOF thin film and second material. This behavior yields a signal transduction for chemical detectors.[15] The tunable and amenable nature of pores within MOFs by the judicious choice of metal clusters and organic linkers offers a potential application for selective gas separation.[20]

Even though different methods have been developed for the syntheses of crystalline nanosized MOFs, including water-in-oil microemulsions,[21,22] surfactant-mediated hydrothermal syntheses,[23] sonochemistry,[24] microwave-assisted routes,[12,25] and coordination modulation,[26,27] the precise control over the size and shape still remains a challenge. For example, the microwave- and ultrasound-assisted approach allows for fabrication of MOF nanocrystals for a short period by heating reaction mixtures under microwave irradiation.[12,24] Although this method is simple and environmentally friendly, it is difficult to tune the size and

Received: September 12, 2011
Revised: October 26, 2011
Published: November 04, 2011

shape of the resulting nanocrystal. In the presence of a surfactant under microwave heating, the synthetic procedure can also alter serendipitously the morphologies of MOF nanocrystals.[25] Using the surfactant-mediated synthetic method, Uemura et al. indicate that organic polymers can be used as inhibitors for the synthesis of coordination polymer nanoparticles,[23] because the protecting polymers can coordinate weakly with metal ions to provide steric stabilization that allows for the formation of nanoparticles. In the case of the reverse-phase microemulsion-based methodology, surfactant molecules can be used for the formation of microemulsion nanodroplets containing metal ions and linkers.[21] The nanodroplets act as microreactors for the formation of MOF nanopaticles. Although this method enables the tuning of the size and shape of nanocrystals by adjusting reaction conditions, it usually leads to the aggregation of the nanocrystals. In some cases, using the reverse-phase microemulsion at room temperature, only amorphous material is produced.[14] The coordination modulation using capping reagents (modulators) with the same functionality of organic linkers enables the impeding of coordination interactions between metal ions and organic linkers to fabricate MOF nanocrystals.[26,27] This modulation allows for the control of the rate of framework extension and crystal growth. Carboxylate-based MOF nanocrystals, such as nanosized MOF-5 colloids[26a] and $[Cu_2(ndc)_2(dabco)_n]$ nanorods (ndc = 1,4-naphthalenedicarboxylate, and dabco = 1,4-diazabicyclo-[2.2.2]octane),[27] are prepared using monocarboxylic acids (*p*-perfluoromethylbenzenecarboxylate) and acetic acid as modulators, respectively.

In this study, we report a new approach for the size-controlled synthesis of uniform carboxylate-based MOF nanocrystals with high crystallinity using simultaneously the non-ionic triblock co-polymer and acetic acid. In this approach, alkylene oxide segments of triblock co-polymer poly(ethylene oxide)−poly-(propylene oxide)−poly(ethylene oxide) (PEO−PPO−PEO) that can coordinate with metal ions[28] play a crucial role in yielding MOF nanocrystals. Acetic acid owning carboxylic functionality that enables the tuning of the rate of the deprotonation of the carboxylic linkers allows us to not only control rationally the size of the MOF nanocrystals but also obtain high crystallinity. Fe−MIL-88B−NH_2 [$Fe_3O(H_2N\text{-}BDC)_3$, with H_2N-BDC = 2-aminoterephtalic acid] as an iron-based MOF nanocystal is selected to illustrate our approach, because this iron-based MOF material is recognized as having a nontoxic nature, highly flexible framework and drug adsorption capacity, and controlled delivery of drugs in the human body.[12] Fe−MIL-88B−NH_2 nanocystals are obtained from iron salts [$FeCl_3$ or $Fe(NO_3)_3$], 2-aminoterephtalic acid, acetic acid, Pluronic F127, and water as synthetic medium. This approach is also expected to achieve other members of MOFs.

EXPERIMENTAL SECTION

Chemicals. $FeCl_3\cdot 6H_2O$ (Aldrich, 97%), $Fe(NO_3)_3\cdot 9H_2O$ (Aldrich, ≥ 98%), H_2N-BDC (Aldrich, 99%), Pluronic F127 ($EO_{97}PO_{69}EO_{97}$, with an average M_n = 12 600, Aldrich), and CH_3COOH (Fisher, 99.7%) were obtained. All chemicals were used as received without further purification.

Synthesis of Fe−MIL-88B−NH_2 Nanocrystals. The size-controlled synthesis of Fe−MIL-88B−NH_2 nanocrystals was accomplished using a hydrothermal route with Fe^{III} salt and 2-aminoterephthalic acid as the metal source and organic linker, respectively, with Pluronic F127 and acetic acid. The reaction mixtures with molar ratios of 1:0.5:1255:*x*:*y* Fe^{3+}/H_2N-BDC/H_2O/F127/CH_3COOH were crystallized for 24 h at 110 °C. The *x* value (F127/Fe^{3+} molar ratio) and *y* value (CH_3COOH/Fe^{3+} molar ratio) were altered to control the size of nanocrystals. In a typical synthesis, 0.16 g of F127 (x = 0.02) was dissolved in 13.34 mL of deionized water and a volume of 1.66 mL of 0.4 M aqueous solution of $FeCl_3\cdot 6H_2O$ (0.66 mmol) was poured into this surfactant solution. The resulting solution was stirred for 1 h before 0.3 mL of acetic acid (y = 8) was injected. After stirring for an additional 1 h, 60 mg (0.33 mmol) of H_2N-BDC was added. The reaction mixture was stirred for 2 h before transferring into an autoclave for the crystallization. The dark brown solid product was recovered and washed several times with ethanol by centrifugation to remove the surfactant and excess reactants. To investigate the effect of the F127/Fe^{3+} molar ratio (x value) and CH_3COOH/Fe^{3+} molar ratio (y value) on the crystal size, the x and y values were tuned from 0.01 to 0.16 and from 0 to 16, respectively. The yield of the reactions was approximately 61% based on H_2N-BDC. For comparison, the Fe−MIL-88B−NH_2 microcrystals were also prepared under the same synthetic conditions, except that both F127 and acetic acid were not added.[29]

Characterization Methods. Transmission electron microscopy (TEM) images were obtained using a JEOL JEM 1230 microscope operating at 120 kV. Samples for TEM measurements were prepared by depositing a drop of the dispersions of the products in absolute ethanol onto carbon-coated copper grids (200 mesh). The excess of the solvent was wicked away with filter paper, and the grids were dried in air. The mean sizes of nanocrystals were determined from statistic distributions evaluated according to TEM images on 100 particles. Scanning electron microscopy (SEM) images were taken on a JEOL 6360 instrument at an accelerating voltage of 3 kV. Powder X-ray diffraction (XRD) patterns were collected on a Bruker SMART APEX II X-ray diffractometer with Cu Kα radiation (λ = 1.5406 Å) in the 2θ range of 5−20° at a scan rate of 1.0° min^{-1}. All samples were dried at 100 °C overnight to remove guest solvent molecules within the pores before the XRD scan. Fourier transform infrared (FTIR) spectra were recorded on a FTS 45 spectrophotometer in the spectral range of 4000−400 cm^{-1} using the KBr disk method. Thermogravimetric analysis (TGA) was carried out with a TGA/SDTA 851^e thermogravimetric analyzer from room temperature to 600 °C with a heating rate of 5 °C min^{-1} under an air flow of 50 mL min^{-1}. ζ-Potential measurements were performed with a Zetasizer Nano ZS in water at 25 °C.

RESULTS AND DISCUSSION

Different stages for the synthesis of Fe−MIL-88B−NH_2 (i) without and (ii) with triblock co-polymer F127 and (iii) with the simultaneous presence of Pluronic F127 and acetic acid in the synthetic mixture were studied to illustrate the role of F127 and acetic acid in the control over the size of Fe−MIL-88B−NH_2. Figure 1 shows electron microscopy images of Fe−MIL-88B−NH_2 samples prepared without and with triblock co-polymer F127. In the synthesis without Pluronic F127, using the method described in ref 29, Fe−MIL-88B−NH_2 microsized crystals were produced from an aqueous reaction mixture of $FeCl_3\cdot 6H_2O$ and H_2N-BDC, with the morphology of bipyramidal hexagonal prism and size of 3.5 μm in length and 1.2 μm in width (Figure 1a). Under the same synthetic conditions, however, in the presence of triblock co-polymer F127, Fe−MIL-88B−NH_2 nanocrystals were obtained. Even though the particle size decreases from micro- to nanometers in the presence of F127, the morphology of the bipyramidal hexagonal prism still remains unchanged (panels a and b of Figure 1).[12,30] Furthermore, when the F127/Fe^{3+} molar ratio varies from 0.01 to 0.04, no significant change in the size of nanocrystals was found (panels b−d of

Figure 1); the average size of the nanocrystals is 50 ± 5 nm in length and 30 ± 5 nm in width. However, when the molar ratio of F127/Fe^{3+} in the synthetic mixture was above 0.04 (i.e., F127/Fe^{3+} = 0.08 and 0.16), TEM images of these samples exhibit non-uniform nanoparticles. Some big nanocrystals besides small nanocrystals were observed (panels e and f of Figure 1). These results indicate that the triblock co-polymer F127 surfactant plays some role in the preparation of Fe−MIL-88B−NH_2 nanocrystals. However, the size of nanocrystals could not be controlled by adjusting the amount of F127 in the synthetic mixture.

To control the size of Fe−MIL-88B−NH_2 nanocrystals, both Pluronic F127 and acetic acid (CH_3COOH) were introduced into the reaction mixtures. The simultaneous presence of acetic acid and the F127 surfactant in the synthetic solution strongly influences the size and aspect ratio of the bipyramidal hexagonal prism of Fe−MIL-88B−NH_2 nanocrystals. In this study, the F127/Fe^{3+} molar ratio was kept unchanged (x = 0.02); however, the CH_3COOH/Fe^{3+} molar ratio (y value) varies from 4 to 16.

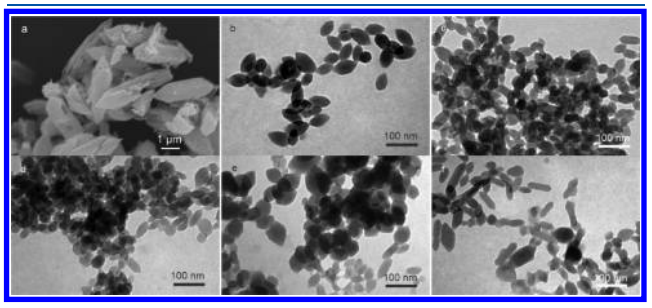

Figure 1. Representative electron microscopy images of different Fe−MIL-88B−NH_2 samples. (a) SEM image of Fe−MIL-88B−NH_2 microcrystals. (b−f) TEM images of Fe−MIL-88B−NH_2 nanocrystals prepared from different F127/Fe^{3+} molar ratios: (b) x = 0.01, (c) x = 0.02, (d) x = 0.04, (e) x = 0.08, and (f) x = 0.16.

Figure 2 shows representative TEM images of Fe−MIL-88B−NH_2 samples obtained from different CH_3COOH/Fe^{3+} molar ratios with the same F127/Fe^{3+} molar ratio of 0.02. Interestingly, the size and aspect ratio of the resulting nanocrystals increase with an increase of the amount of CH_3COOH added in the synthetic mixture. At a low CH_3COOH/Fe^{3+} molar ratio ($y \leq 4$), no significant difference in the size and shape of the nanocrystals was observed (Figure 2a), as compared to those of the nanocrystals prepared without acetic acid (Figure 1c). However, with an increase of the CH_3COOH/Fe^{3+} molar ratio from 4 to 8 and to 16, the size of nanocrystal products increases rapidly from 50 ± 5 to 150 ± 10 and to 500 ± 10 nm in length and from 30 ± 5 to 60 ± 10 and to 150 ± 10 nm in width, respectively; the aspect ratio (length/width) increases from 1.5 to 3.5. The same trend was also observed when $Fe(NO_3)_3 \cdot 9H_2O$ was used as a metal source instead of $FeCl_3 \cdot 6H_2O$ (see Figures S1 and S2 of the Supporting Information). On the contrary, when the CH_3COOH/Fe^{3+} molar ratio was kept unchanged (y = 0.04) but the F127/Fe^{3+} molar ratio (x value) varied from 0.01 to 0.04, the size and shape of the nanocrystals are almost unchanged (see Figure S3 of the Supporting Information). This behavior is similar to that for the case without acetic acid.

Therefore, adjusting the molar ratio of CH_3COOH/Fe^{3+} allows for the control of the size of the nanocrystals. It is obvious that, with a high CH_3COOH/Fe^{3+} molar ratio ($y \geq 8$) in the synthesis mixture, highly well-defined morphologies and isolated Fe−MIL-88B−NH_2 nanocrystals were obtained. This also suggests that a high concentration of acetic acid favors the formation of well-defined crystalline nanocrystals.

In the previous research[27] on the synthesis of carboxylate-based MOF nanocrystals via coordination modulation using acetic acid as the capping reagent (in the absence of the F127 surfactant), the presence of acetic acid allows for the formation of $[Cu_2(ndc)_2(dabco)_n]$ nanorods and the higher concentration of acetic acid leads to the smaller width of the nanorods. In that case,

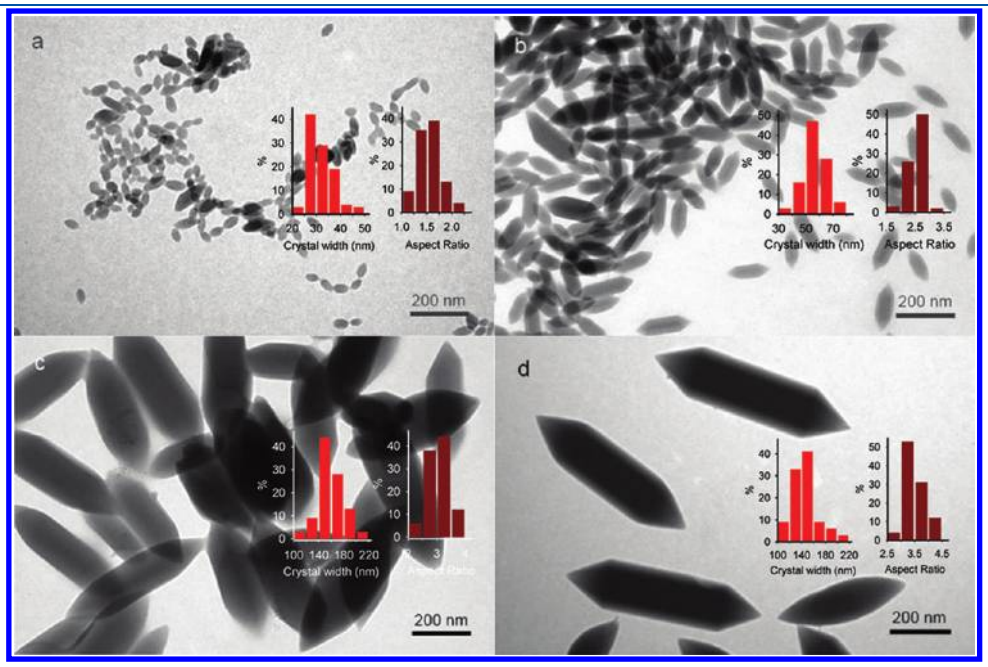

Figure 2. TEM images of Fe−MIL-88B−NH_2 nanocrystal samples prepared with the same F127/Fe^{3+} molar ratio of 0.02 (x = 0.02) for all experiments at different CH_3COOH/Fe^{3+} molar ratios (y = CH_3COOH/Fe^{3+}): (a) y = 4, (b) y = 8, (c) y = 12, and (d) y = 16 (Inset: distributions of the width and aspect ratio of nanocrystals).

dx.doi.org/10.1021/la203570h |*Langmuir* 2011, 27, 15261–15267

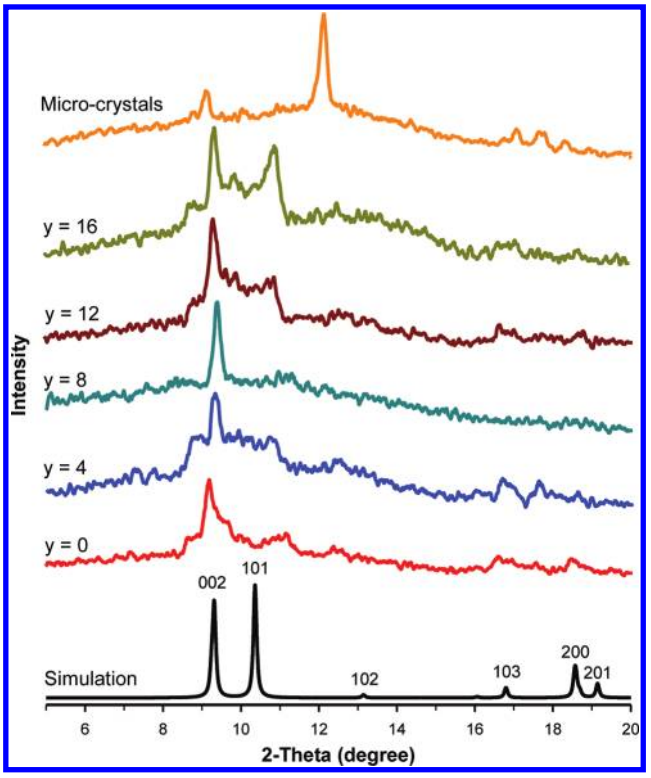

Figure 3. Powder XRD patterns for Fe−MIL-88B−NH_2 nanocrystal samples prepared at different molar ratios of CH_3COOH/Fe^{3+} (y = CH_3COOH/Fe^{3+}) in the presence of surfactant F127 (F127/Fe^{3+} = 0.02) and the microcrystals prepared in the absence of both surfactant F127 and acetic acid. The simulated XRD pattern for the chromium-(III)-based MIL-88B structure created from CIF is also present.[31]

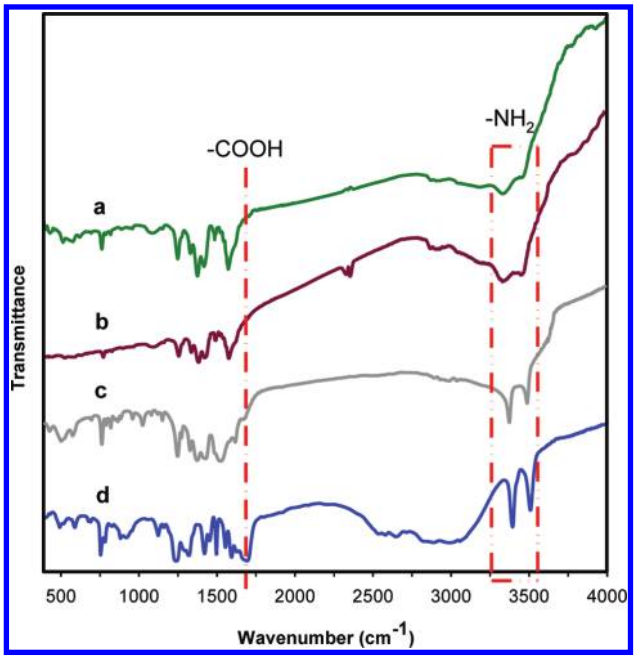

Figure 4. FTIR spectra of Fe−MIL-88B−NH_2 nanocrystals prepared (a) in the presence of both Pluronic F127 and acetic acid with the F127/Fe^{3+} molar ratio of x = 0.02 and CH_3COOH/Fe^{3+} of y = 8, (b) in the presence of Pluronic F127 (x = 0.02) and absence of acetic acid, (c) microcrystals, and (d) free 2-aminoterephthatic acid.

acetic acid competes with the dicarboxylic linker (1,4-naphthalene dicarboxylic acid) to coordinate with dicopper clusters to create nanocrystals. A larger amount of acetic acid can passivate a larger fraction of external surface area, resulting in smaller nanocrystals. On the contrary, in this work, for the synthesis of Fe−MIL-88B−NH_2 crystals, the presence of acetic acid (without the F127 surfactant) in the synthetic mixture led to the formation of Fe−MIL-88B−NH_2 microsized crystals (see Figure S4 of the Supporting Information). This could be mainly due to the difference in the synthesis medium: the aqueous medium for Fe−MIL-88B−NH_2 instead of the organic solvent for $[Cu_2(ndc)_2(dabco)_n]$.

Furthermore, in the simultaneous presence of F127 and acetic acid, nanosized Fe−MIL-88B−NH_2 crystals were obtained. The nanosize of Fe−MIL-88B−NH_2 increases with a increase of the concentration of acetic acid in the synthetic mixture. These results suggest a different behavior of acetic acid in the formation of the Fe−MIL-88B−NH_2 crystals in the presence of the F127 surfactant. In this case, triblock co-polymer F127 plays an important role in the formation of MOF nanocrystals because of its ability to coordinate with metal ions,[28] while acetic acid tailors the size of nanocrystals by controlling the deprotonation of carboxylic linkers during synthesis.

Figure 3 shows the powder XRD patterns for the Fe−MIL-88B−NH_2 nanocrystal samples prepared with various molar ratios of CH_3COOH/Fe^{3+} (y = 0−16) in the presence of surfactant F127 (F127/Fe^{3+} = 0.02) and the microcrystal sample prepared in the absence of both triblock co-polymer F127 and acetic acid. As a reference, the simulated XRD pattern for the chromium-(III)-based MIL-88B structure (denoted as Cr−MIL-88B) created from the crystallographic information file (CIF) is also present.[31] As seen in Figure 3, the XRD reflections of the nanocrystal samples match those of the simulated XRD pattern of Cr−MIL-88B, readily indexing hexagonal space group $P6_3/mmc$ of the MIL-88B structure of the synthesized nanocrystals.[29,31,32] On the basis of the Bragg peak positions, the calculated unit cell parameters of the dried forms of all nanocrystals are $a \sim 9.7$ Å and $c \sim 19.0$ Å, which are similar to those of the anhydrous form of Cr-MIL-88B ($a \sim 9.6$ Å, and $c \sim 19.1$ Å).[31,33] The intensity of the diffraction peaks for the nanocrystals increases with an increasing CH_3COOH/Fe^{3+} molar ratio, suggesting that, with a higher amount of acetic acid in the synthetic mixture, a higher crystallinity of the samples can be obtained. This is consistent with the morphologies observed by TEM images. This also suggests the role of acetic acid in the improvement of the crystallinity of the nanocrystals.

The XRD pattern for the Fe−MIL-88B−NH_2 microcrystals exhibits the diffraction peak with the highest intensity at 2θ of 12.2. It is noted that the slight discrepancies in intensity and the 2θ position of the reflections are due to the structural flexibility of MIL-88B.[29,30,33] Because of the structural flexibility, the guest species (organic and/or inorganic species) in the pore channels can lead to the motions of the skeleton accompanied by the position shift as well as the change in intensity of the reflections. The magnitude of the motion is strongly affected by the degree of pore-filling and the nature of the guests.[33−35] Generally, it is difficult to remove completely guest molecules within the pore channels of large MOF crystals (microsize) compared to those in small MOF crystals (nanosize), because of longer diffusion pathways. Furthermore, the shifted position of the reflections, as seen in Figure 3, is presumably attributed to the effect of the crystal size of Fe−MIL-88B−NH_2.

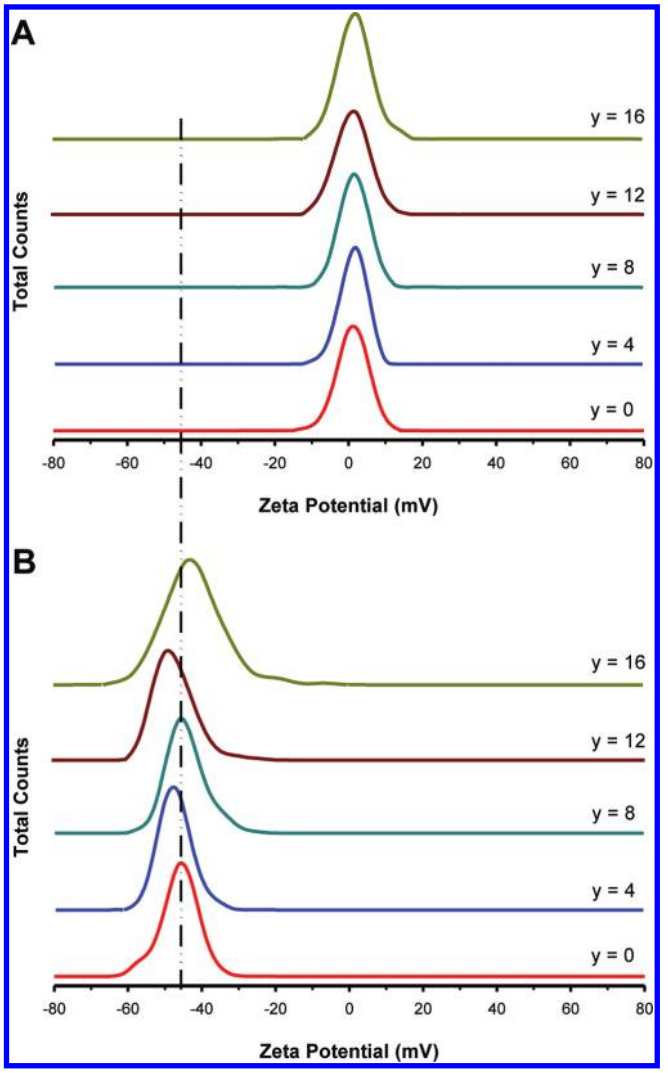

Figure 5. ζ-Potential distributions in aqueous solution at pH ∼7 of a series of Fe−MIL-88B−NH_2 nanocrystals prepared from $FeCl_3 \cdot 6H_2O$ with different CH_3COOH/Fe^{3+} molar ratios ($y = CH_3COOH/Fe^{3+}$) at the same $F127/Fe^{3+}$ molar ratio of 0.02 ($x = 0.02$) (A) before and (B) after washing.

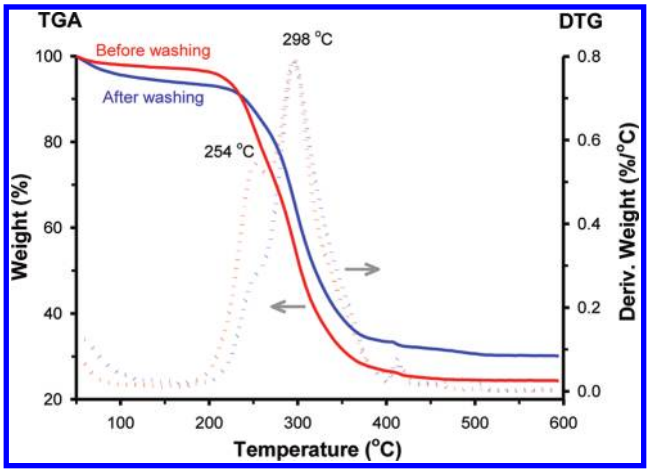

Figure 6. TGA curves (solid) and their first DTG curves (dotted) for Fe−MIL-88B−NH_2 nanocrystals prepared with the CH_3COOH/Fe^{3+} molar ratio of $y = 8$ and the $F127/Fe^{3+}$ molar ratio of $x = 0.02$ before (red) and after (blue) washing.

To identify the presence of amino groups in the resulting nanocrystals, FTIR spectra for different Fe−MIL-88B−NH_2 samples were recorded. Curves a and b of Figure 4 show FTIR spectra for the nanocrystal samples prepared in the presence of both Pluronic F127 ($F127/Fe^{3+} = 0.02$) and acetic acid ($CH_3COOH/Fe^{3+} = 8$) and in the presence Pluronic F127, however, in the absence of acetic acid, respectively. For comparison, FTIR spectra for the Fe−MIL-88B−NH_2 microcrystals (Figure 4c) and free 2-aminoterephthalic acid linker (Figure 4d) are also presented. In general, the samples of Fe−MIL-88B−NH_2 nano- and microcrystals exhibit similar FTIR spectra (curves a−c of Figure 4). Two bands at around 3490 and 3370 cm^{-1}, which are attributed to the symmetric and asymmetric stretching absorptions of primary amine groups, were observed. These FTIR bands correspond to those of free 2-aminoterephthalic acid (Figure 4d), indicating the amino groups in the nanoscale MOF crystals.[36] No band at around 1700 cm^{-1} that is characteristic of protonated carboxylic groups was observed in curves a and b of Figure 4, suggesting the absence of protonated carboxylic groups (because of acetic acid) in the nanocrystals.[37] This also indicates that most acetic acid was removed from the nanocrystals upon washing. It can be concluded that the introduction of acetic acid during the synthesis did not affect amine groups in the nanocrystal products.

To identify the presence of the surfactant on the surface of the nanocrystal products after the synthesis, ζ-potential measurements were carried out in the neutral aqueous solution (pH ∼7) for a series of Fe−MIL-88B−NH_2 nanocrystals prepared with different CH_3COOH/Fe^{3+} molar ratios in the presence of the F127 surfactant before washing (i.e., the product obtained after removing the mother liquors without further purification) and after washing with ethanol. The ζ-potential curves of these samples are shown in Figure 5. Before washing, in aqueous solution (at pH ∼7), for all samples, no charge essential on the surface of nanoparticles was observed. The ζ potential of these samples is close to the zero point of charge (ZPC) (Figure 5A). No charge before washing could be attributed to non-ionic copolymer F127 capped on the nanocrystal surface. However, upon washing several times with ethanol, in the aqueous solution at the same pH ∼7, these samples exhibit negative charges, which vary in the range of −41 and −51 mV (Figure 5B). The Fe−MIL-88B−NH_2 structure $[Fe_3O(solvent)_3Cl(NH_2\text{-}BDC)_3 \cdot m\text{solvent}]$ is constructed from the trimers of μ_3-O-bridged Fe^{III} octahedra $[Fe_3O(COO)_6]$, which are connected by 2-aminoterephtalic acid. Each Fe^{III} trimer needs a Cl^- counteranion to maintain electric neutrality. Chlorine anions are attributed to such a negative potential. This also indicates that most of the surfactant was removed from the particle surface upon washing.

TGA and derivative thermogravimetric (DTG) curves of the Fe−MIL-88B−NH_2 nanocrystal sample prepared with the CH_3COOH/Fe^{3+} molar ratio of 8 and $F127/Fe^{3+}$ molar ratio of 0.02 before and after washing are shown in Figure 6. Both samples exhibit similar TGA−DTG profiles, but some results show the presence of the surfactant in the material before washing. The TGA curves exhibit a major weight loss in the range of 200−400 °C with two maximum peaks at 254 and 298 °C (see DTG curves). The former is consistent with the decomposition temperature of Pluronic F127,[38] implying the presence of the F127 surfactant in the materials. The latter is

Scheme 1. Schematic Representation for the Size-Controlled Fabrication of Fe−MIL-88B−NH_2 Nanocrystals

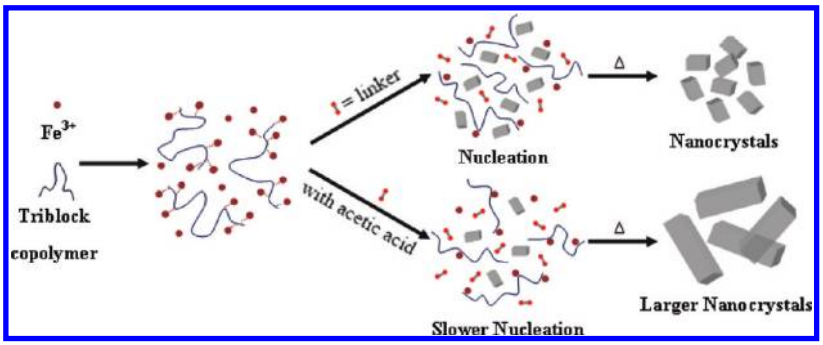

attributed mainly to the MOF structure decomposition.[39] It is noted that the intensity of the peak at 254 °C and the weight loss in the temperature range of 200−265 °C for the Fe−MIL-88B−NH_2 nanocrystals before washing are much higher than those for this nanocrystal after washing, suggesting that most of the F127 surfactant was removed. The difference in the weight loss of this sample before and after washing was about 10 wt %.

The size-controlled formation of Fe−MIL-88B−NH_2 nanocrystals in the presence of Pluronic F127 and acetic acid can be explained by the fact that the alkylene oxide segments of the triblock co-polymer enable the weak coordination with metal ions.[28] Therefore, the presence of the triblock co-polymer leads to the stabilization of MOF nuclei at the early stage of the synthesis. The subsequent crystal growth may involve the Ostwald ripening at the expense of metal ions and linkers as well as smaller nanoparticles to yield MOF nanocrystals. The formation of large nanoparticles at the cost of small nanoparticles is presumably due to the energy difference between large and small nanoparticles.[40] Besides, the nucleation and growth of MOF nanocrystals could occur within the mesophases of F127 that act as nanoreactors.[41] Furthermore, the nucleation and crystal growth can be affected by the presence of acetic acid. There is indeed a competitive interaction of dicarboxylic linkers and acetic acid with iron ions during the nucleation and crystal growth processes. It is shown that the formation of carboxylate-based MOFs is primarily dependent upon the degree of deprotonation of carboxylic linkers.[26a] The amount of acetic acid could control the degree of deprotonation of carboxylic linkers. A higher CH_3COOH/Fe^{3+} molar ratio (i.e., a higher concentration of acetic acid) leads to a lower degree of deprotonation of the H_2N-BDC linker, and thus, the rate of nucleation and crystal growth could be slower, resulting in bigger MOF nanocrystals.[22,42] The size-controlled fabrication of Fe−MIL-88B−NH_2 nanocrystals is illustrated by Scheme 1.

Upon adding H_2N-BDC (linker molecules) into the aqueous solution containing the F127 surfactant and iron(III) salt, even at room temperature, dark precipitates immediately appeared, indicating a rapid formation of Fe−MIL-88B−NH_2 framework units, whereas this phenomenon was not observed in the reaction mixture without F127 under the same synthesis conditions. In the presence of acetic acid, a slower change in color from yellow for the linker molecules to dark for MOF species in the early stage was also observed because of the slow cost of linker molecules for the MOF formation.

The aspect ratio of nanocrystals is also controlled by the acetic acid concentration. The aspect ratio increases with an increase of the molar ratio of CH_3COOH/Fe^{3+} (Figure 2). At a molar ratio of CH_3COOH/Fe^{3+} equal or higher than 8, the growth of nanocrystals along the [001] direction corresponding to the length of nanocrystals is preferable.[30] Because all 2-aminoterephthalic acid molecules are oriented along the [001] direction,[30] the interaction between metal ions and the carboxylic groups of linker molecules along the [001] direction is more favorable than others, resulting in faster growth. However, at low concentrations of acetic acid or without acetic acid in the presence of the triblock co-polymer F127 surfactant, no significant change in the size and aspect ratio of the nanocrystals is observed even with high F127 concentrations (Figure 1), indicating the same effect of the F127 surfactant in all directions during the crystal growth.

CONCLUSION

We have demonstrated a new route to the synthesis of Fe−MIL-88B−NH_2 nanocrystals with controlled sizes and aspect ratios using simultaneously the triblock co-polymer and acetic acid in the synthetic mixture. The alkylene oxide segments of the triblock co-polymer enable the coordination with metal ions and stabilization of MOF nuclei in the early stage and have a key role in yielding uniform MOF nanocrystals. The size and aspect ratio of nanocrystals can be adjusted by altering the amount of acetic acid in the synthetic mixture. Acetic acid can control the degree of deprotonation of carboxylic linkers. A higher concentration of acetic acid leads to a lower degree of deprotonation of the H_2N-BDC linker and, thus, a lower rate of nucleation and crystal growth, resulting in larger MOF nanocrystals. This allows for the tailoring of the crystal size from a few tenths to a few hundredths of nanometers and the aspect ratio. We believe that this approach can be extended to other carboxylate-based MOF nanocrystals. These nanocrystal materials have potential applications in different fields, such as catalysis, chemical sensors, and related advanced nanodevices, because of the nanoscale size, short diffusion pathways, and more exposed active sites.

ASSOCIATED CONTENT

Supporting Information. TEM images (Figure S1), XRD pattern of Fe−MIL-88B−NH_2 nanocrystals prepared from $Fe(NO_3)_3 \cdot 9H_2O$ (Figure S2), TEM images of Fe−MIL-88B−NH_2 nanocrystals prepared at the same CH_3COOH/Fe^{3+} molar ratio with different $F127/Fe^{3+}$ molar ratios (Figure S3), and SEM image of the microcrystals prepared from the synthetic mixture containing $FeCl_3 \cdot 6H_2O$, H_2N-BDC, and acetic acid

(CH_3COOH/Fe^{3+} = 8) (Figure S4). This material is available free of charge via the Internet at http://pubs.acs.org.

AUTHOR INFORMATION

Corresponding Author
*E-mail: trong-on.do@gch.ulaval.ca.

ACKNOWLEDGMENT

We thank the Natural Sciences and Engineering Research Council of Canada (NSERC, Ottawa, Ontario, Canada), the Centre de Recherche sur les Propriétés des Interfaces et de Catalyse (CERPIC, Laval University, Quebec City, Quebec, Canada), and the Centre in Green Chemistry and Catalysis (CGCC, Montreal, Quebec, Canada) for financial support and the Vietnam Ministry of Education and Training for a scholarship (to Minh-Hao Pham).

REFERENCES

(1) (a) Férey, G. *Chem. Soc. Rev.* **2008**, *37*, 191–214. (b) Corma, A.; García, H.; Llabrés i Xamena, F. X. *Chem. Rev.* **2010**, *110*, 4606–4655. (c) Tanabe, K. K.; Cohen, S. M. *Chem. Soc. Rev.* **2011**, *40*, 498–519. (d) Horike, S.; Kitagawa, S. In *Metal−Organic Frameworks: Applications from Catalysis to Gas Storage*; Farrusseng, D., Eds.; Wiley-VCH: New York, 2011; p 3. (e) Férey, G.; Serre, C.; Devic, T.; Maurin, G.; Jobic, H.; Llewellyn, P. L.; Weireld, G. D.; Vimont, A.; Daturi, M.; Chang, J.-S. *Chem. Soc. Rev.* **2011**, *40*, 550–562.

(2) (a) Furukawa, H.; Ko, N.; Go, Y. B.; Aratani, N.; Choi, S. B.; Choi, E.; Yazaydin, A. Ö.; Snurr, R. Q.; O'Keeffe, M.; Kim, J.; Yaghi, O. M. *Science* **2010**, *329*, 424–428. (b) Li, Q.; Zhang, W.; Miljanic, O. Š.; Sue, C.-H.; Zhao, Y.-L.; Liu, L.; Knobler, C. B.; Stoddart, J. F.; Yaghi, O. M. *Science* **2009**, *325*, 855–859. (c) Hasegawa, S.; Horike, S.; Matsuda, R.; Furukawa, S.; Mochizuki, K.; Kinoshita, Y.; Kitagawa, S. *J. Am. Chem. Soc.* **2007**, *129*, 2607–2614. (d) Seo, J.; Bonneau, C.; Matsuda, R.; Takata, M.; Kitagawa, S. *J. Am. Chem. Soc.* **2011**, *133*, 9005–9013.

(3) Vuong, G. T.; Do, T. O. *J. Am. Chem. Soc.* **2007**, *129*, 3810–3811.

(4) Do, T. O.; Kaliaguine, S. *Angew. Chem., Int. Ed.* **2001**, *40*, 3248–3251.

(5) Férey, G.; Mellot-Draznieks, C.; Serre, C.; Millange, F.; Dutour, J.; Surblé, S.; Margiolaki, I. A. *Science* **2005**, *309*, 2040–2042.

(6) Koh, K.; Wong-Foy, A. G.; Matzger, A. J. *J. Am. Chem. Soc.* **2009**, *131*, 4184–4185.

(7) Koh, K.; Wong-Foy, A. G.; Matzger, A. J. *Angew. Chem., Int. Ed.* **2008**, *47*, 677–680.

(8) (a) Furukuwa, H.; Ko, N; Go, Y. B.; Aratani, N.; Choi, S. B.; Choi, E.; Yazaudin, A. Ö.; Snurr, R. Q.; O'Keeffe, M.; Kim, J.; Yaghi, O. M. *Science* **2010**, *329*, 424–428. (b) Klein, N.; Semkovska, I.; Gedrich, K.; Stoeck, U.; Henschel, A.; Mueller, U.; Kaskel, S. *Angew. Chem., Int. Ed.* **2009**, *48*, 9954–9957.

(9) (a) Eddaoudi, M.; Kim, J.; Rosi, N.; Vodak, D.; Wachter, J.; O'Keeffe, M.; Yaghi, O. M. *Science* **2002**, *295*, 469–472. (b) Jiang, H.-L.; Tatsu, Y.; Lu, Z.-H.; Xu, Q. *J. Am. Chem. Soc.* **2010**, *132*, 5586–5587.

(10) Farha, O. K.; Malliakas, C. D.; Kanatzidis, M. G.; Hupp, J. T. *J. Am. Chem. Soc.* **2010**, *132*, 950–952.

(11) Zhao, Y.; Zhang, J.; Han, B.; Song, J.; Li, J.; Wang, Q. *Angew. Chem., Int. Ed.* **2011**, *50*, 636–639.

(12) Horcajada, P.; Chalati, T.; Serre, C.; Gillet, B.; Sebrie, C.; Baati, T.; Eubank, J. F.; Heurtaux, D.; Clayette, P.; Kreuz, C.; Chang, J. S.; Hwang, Y. K.; Marsaud, V.; Bories, P. N.; Cynober, L.; Gil, S.; Férey, G.; Couvreur, P.; Gref., R. *Nat. Mater.* **2010**, *9*, 172–178.

(13) McKinlay, A. C.; Morris, R. E.; Horcajada, P.; Férey, G.; Gref, R.; Couvreur, P.; Serre, C. *Angew. Chem., Int. Ed.* **2010**, *49*, 6260–6266.

(14) Rieter, W. J.; Taylor, K. M. L.; An, H.; Lin, W.; Lin, W. *J. Am. Chem. Soc.* **2006**, *128*, 9024–9025.

(15) Allendorf, M. D.; Houk, R. J. T.; Andruszkiewicz, L.; Talin, A. A.; Pikarsky, J.; Choudhury, A.; Gall, K. A.; Hesketh, P. J. *J. Am. Chem. Soc.* **2008**, *130*, 14404–14405.

(16) Nune, S. K.; Thallapally, P. K.; Dohnalkova, A.; Wang, C.; Liu, J.; Exarhos, G. J. *Chem. Commun.* **2010**, *46*, 4878–4880.

(17) Uemura, T.; Kitagawa, S. *Chem. Lett.* **2005**, *34* (2), 132–137.

(18) Horcajada, P.; Serre, C.; Grosso, D.; Boissière, C.; Perruchas, S.; Sanchez, C.; Férey, G. *Adv. Mater.* **2009**, *21*, 1931–1935.

(19) Rieter, W. J.; Taylor, K. M. L.; Lin, W. *J. Am. Chem. Soc.* **2007**, *129*, 9852–9853.

(20) Li, J. R.; Kuppler, R. J.; Zhou, H. C. *Chem. Soc. Rev.* **2009**, *38*, 1477–1504.

(21) Tanaka, D.; Henke, A.; Albrecht, K.; Moeller, M.; Nakagawa, K.; Kitagawa, S.; Groll, J. *Nat. Chem.* **2010**, *2*, 410–416.

(22) Diring, S.; Furukawa, S.; Takashima, Y.; Tsuruoka, T.; Kitagawa, S. *Chem. Mater.* **2010**, *22*, 4531–4538.

(23) (a) Uemura, T.; Kitagawa, S. *J. Am. Chem. Soc.* **2003**, *125*, 7814–7815. (b) Uemura, T.; Ohba, M.; Kitagawa, S. *Inorg. Chem.* **2004**, *43*, 7339–7345.

(24) Qiu, L. G.; Li, Z. Q.; Wu, Y.; Wang, W.; Xu, T.; Jiang, X. *Chem. Commun.* **2008**, 3642–3644.

(25) Taylor, K. M. L.; Jin, A.; Lin, W. *Angew. Chem.* **2008**, *120*, 7836–7839.

(26) (a) Hermes, S.; Witte, T.; Hikov, T.; Zacher, D.; Bahnmuller, S.; Langstein, G.; Huber, K.; Fischer, R. A. *J. Am. Chem. Soc.* **2007**, *129*, 5324–5325. (b) Horcajada, P.; Serre, C.; Grosso, D.; Boissiere, C.; Perruchas, S.; Sanchez, C.; Férey, G. *Adv. Mater.* **2009**, *21*, 1931–1935. (c) Guo, H.; Zhu, Y.; Qiu, S.; Lercher, J. A.; Zhang, H. *Adv. Mater.* **2010**, *22*, 4190–4192.

(27) Tsuruoka, T.; Furukawa, S.; Takashima, Y.; Yoshida, K.; Isoda, S.; Kitagawa, S. *Angew. Chem., Int. Ed.* **2009**, *48*, 4739–4743.

(28) Bailey, F. E. Jr.; Koleske, J. V. *Alkylene Oxides and Their Polymers*; Marcel Dekker: New York, 1990.

(29) Bauer, S.; Serre, C.; Devic, T.; Horcajada, P.; Marrot, J.; Férey, G.; Stock, N. *Inorg. Chem.* **2008**, *47*, 7568–7576.

(30) Scherb, C.; Schodel, A.; Bein, T. *Angew. Chem., Int. Ed.* **2008**, *47*, 5777–5779.

(31) Surblé, S.; Serre, C.; Mellot-Draznieks, C.; Millange, F.; Férey, G. *Chem. Commun.* **2006**, 284–286.

(32) Serre, C.; Millange, F.; Surbé, S.; Férey, G. *Angew. Chem., Int. Ed.* **2004**, *43*, 6286–6289.

(33) Serre, C.; Mellot-Draznieks, C.; Surblé, S.; Audebrand, N.; Filinchuk, Y.; Férey, G. *Science* **2007**, *315*, 1828–1831.

(34) Jahan, M.; Bao, Q.; Yang, J. X.; Loh, K. P. *J. Am. Chem. Soc.* **2010**, *132*, 14487–14495.

(35) Hafizovic, J.; Bjorgen, M.; Olsbye, U.; Dietzel, P. D. C.; Bordiga, S.; Prestipino, C.; Lamberti, C.; Lillerud, K. P. *J. Am. Chem. Soc.* **2007**, *129*, 3612–3620.

(36) Gascon, J.; Aktay, U.; Hernandez-Alonso, M. D.; van Klink, G. P. M.; Kapteijn, F. *J. Catal.* **2009**, *261*, 75–87.

(37) Chen, W.; Wang, J. Y.; Chen, C.; Yue, Q.; Yuan, H. M.; Chen, J. S.; Wang, S. N. *Inorg. Chem.* **2003**, *42*, 944–946.

(38) Jiua, J.; Kurumadac, K.; Peib, L.; Tanigakia, M. *Colloids Surf., B* **2004**, *38*, 121–125.

(39) Gaudin, C.; Cunha, D.; Ivanoff, E.; Horcajada, P.; Chevé, G.; Yasri, A.; Loget, O.; Serre, C.; Maurin, G. *Microporous Mesoporous Mater.* **2011**, DOI: 10.1016/j.micromeso.2011.06.011.

(40) Tang, J.; Alivisatos, A. P. *Nano Lett.* **2006**, *6*, 2701–2706.

(41) (a) Braun, P. V.; Osenar, P.; Stupp, S. I. *Nature* **1996**, *380*, 325–328. (b) Dellinger, T. M.; Braun, P. V. *Chem. Mater.* **2004**, *16*, 2201–2207. (c) Wang, C.; Chen, D.; Jiao, X. *Sci. Technol. Adv. Mater.* **2009**, *10*, No. 023001.

(42) Uemura, T.; Hoshino, Y.; Kitagawa, S.; Yoshida, K.; Isoda, S. *Chem. Mater.* **2006**, *18*, 992–995.

Supporting Information

A Novel Route to Size-Controlled Fe-MIL-88B-NH_2 Metal-Organic Framework Nanocrystals

Minh-Hao Pham[†], *Gia-Thanh Vuong*[†], *Anh-Tuan Vu*[‡] *and Trong-On Do*[†]*

[†]Department of Chemical Engineering, Laval University, Quebec, G1V 0A6, CANADA; [‡]Institute of Chemistry, Vietnamese Academy of Science and Technology

[*]Corresponding author. E-mail: Trong-On.Do@gch.ulaval.ca

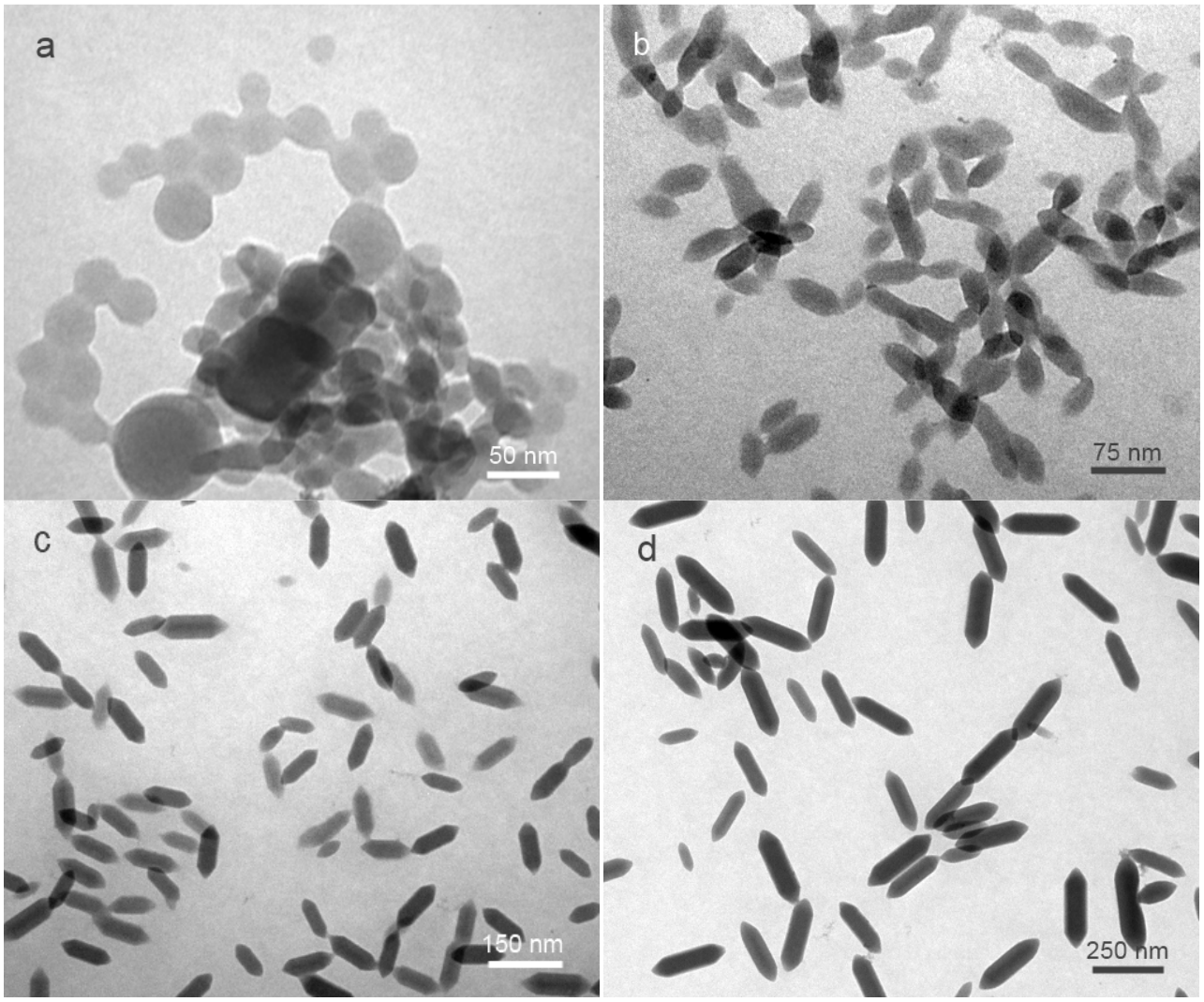

Figure S1. TEM images of Fe-MIL-88B-NH_2 nanocrystals prepared from $Fe(NO_3)_3.9H_2O$ at different molar ratios of CH_3COOH/Fe^{3+} (y = CH_3COOH/Fe^{3+}), while keeping the same $F127/Fe^{3+}$ molar ratio of 0.02 (x = 0.02): (a) y = 0, (b) y = 8, (c) y = 12 and (d) y = 16.

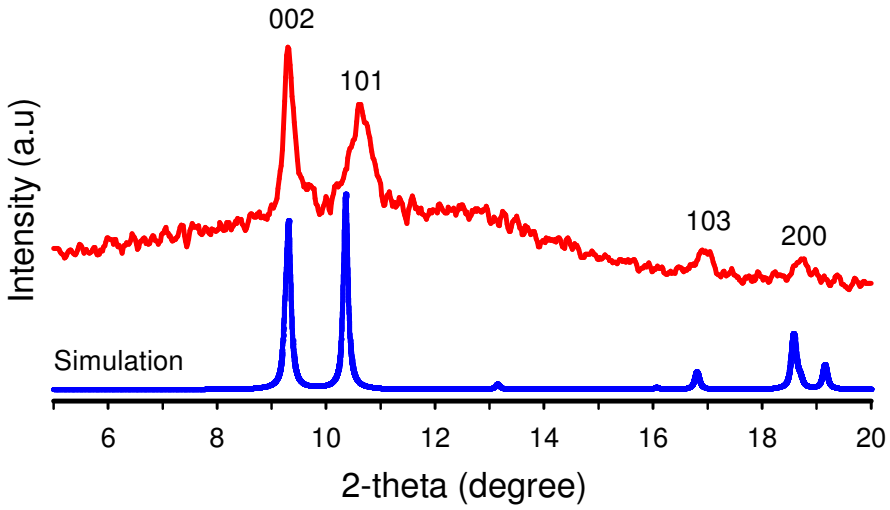

Figure S2. Powder XRD pattern for Fe-MIL-88B-NH_2 nanocrystals prepared from $Fe(NO_3)_3.9H_2O$ at CH_3COOH/Fe^{3+} = 12 and $F127/Fe^{3+}$ = 0.02 (red line), and the simulated XRD pattern for chromium (III)-based MIL-88B structure (blue line).

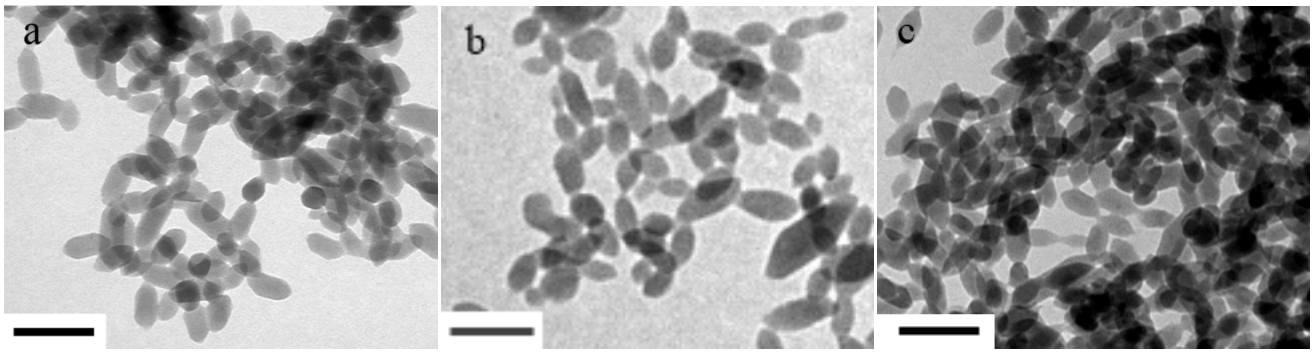

Figure S3. TEM images of Fe-MIL-88B-NH_2 nanocrystals prepared at the same CH_3COOH/Fe^{3+} molar ratio of 4 (y = 4) with different $F127/Fe^{3+}$ molar ratios: (a) x = 0.01, (b) x = 0.02 and (c) x = 0.04. The scale bar is 100 nm.

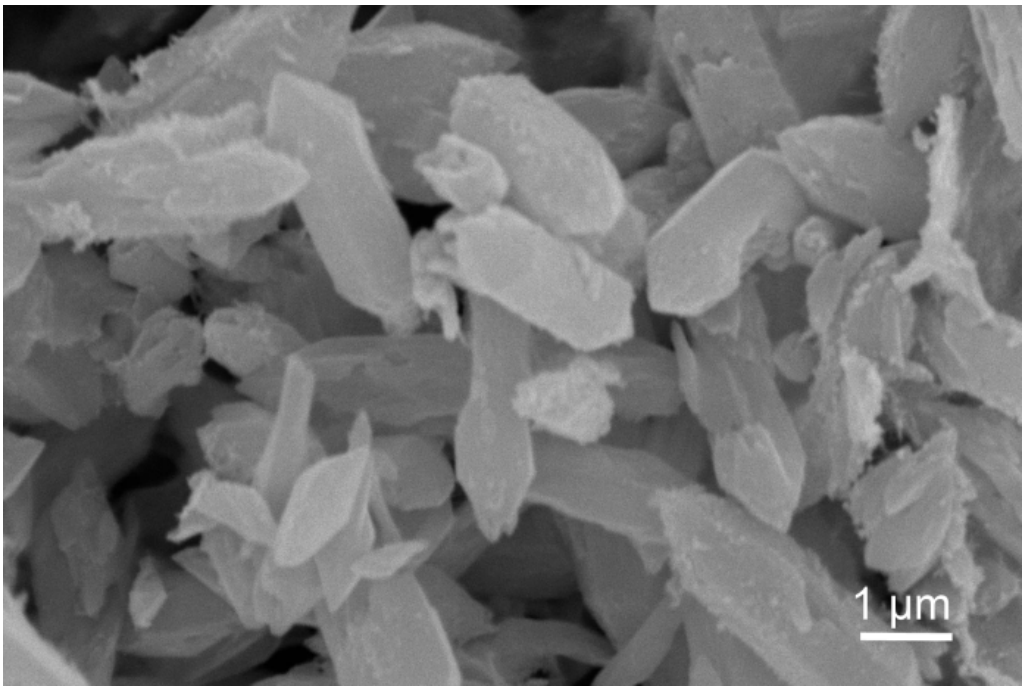

Figure S4. SEM image of Fe-MIL-88B-NH_2 micro-crystals prepared from the synthetic mixture containing $FeCl_3.6H_2O$, H_2N-BDC and acetic acid (CH_3COOH/Fe^{3+} = 8) without F127 surfactant.